Unique Modular Structure of Multicell High-Boost Converters With Reduced Component Currents

Guidong Zhang, *Member, IEEE*, Zhiyang Wang, Herbert Ho-Ching Iu, *Senior Member, IEEE*, Si-Zhe Chen, Yuanmao Ye, *Member, IEEE*, Bo Zhang, *Senior Member, IEEE*, and Yun Zhang

***Abstract*—The traditional switched-inductor technique for high-step-up conversion is widely utilized in industrial applications, especially multicell technique is combined to realize ultra-high voltage. However, the component currents are accordingly increasing with the increasing number of cells, which results in high cost, low efficiency, and low stability. In order to solve these problems, an improved multicell structure of switched inductor is devised, which can be utilized to replace traditional switched-inductor cells for higher actual boost ratio and lower diode currents. An example of the proposed structure-based boost converter is demonstrated for a detailed analysis, and it is followed with a comparison to verify its features. Finally, simulations and experiments are conducted to validate the effectiveness.**

***Index Terms*—High step-up, multicell, reduced component currents, switched inductor.**

I. Introduction

In RECENT years, air pollution and energy shortage have attracted major national attentions because of some environmental phenomena affecting human life and safety [1], [2]. To solve these problems, the worldwide-installed renewable energy capacity shows nearly an exponential increase due to decrease in costs and improvements in renewable energy techniques, which raises higher demands on power electronics techniques, especially the high-step-up energy conversion, i.e., to boost a very low voltage to a grid-connected one [3], [4].

In practice, the basic boost converter can only realize a very limited voltage gain due to its instincts topology and the parasitic parameters, so it cannot fulfill the requirements in renewable energy system [5]. A cascaded boost converter is also capable of providing high voltage gain but with many switches and high switch voltage stresses [6], [7]. Power converter topologies employed in renewable generation systems, such as photovoltaic arrays or fuel cells, are mainly characterized by multistage converters, which also results in too many switches and control units [8], [9].

In order to solve these problems, there are various high-step-up techniques coined out in the literatures, including novel cells, i.e., switched inductor (SL) [10], [11], switched capacitor (SC) [12], active switched-inductor (A-SL) [13], Z-source [14], [15], and Y-source [16]; connections techniques, i.e., cascaded [17], output series [18], interleaved [19], [20], and multicell [21], [22]; and some combinations of them. Their features are concluded in Tables I and II, respectively.

TABLE I
High-Voltage-Gain Cells

Type	Structure	Feature
SL	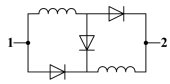	• Low Capacity • Low Loss • Small Size • Low Cost • Simple Control
SC	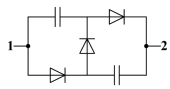	• Simple Modulalization • Voltage Multiply • Low Cost • Simple Control • Stable
A-SL	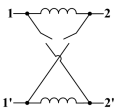	• Low Switch Stress • Many Switches • Uncommon-Grounded Ports • Complex Control • High Cost
Z-source	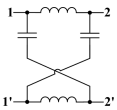	• Large Size • For Inversion • High Component Stress
Y-source	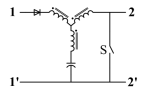	• High Voltage Gain • Large Size • High Cost • High Component Stress

Manuscript received August 27, 2017; revised October 9, 2017; accepted October 31, 2017. Date of publication November 6, 2017; date of current version June 22, 2018. This work was supported in part by the National Natural Science Foundation of China under Grant U1501251 and Grant 51307025, in part by the Natural Science Foundation of Guangdong Province under Grant 2017A030310243 and Grant 2017B030312001, and in part by the Foundation for Distinguished Young Talents in Higher Education of Guangdong under Grant 2016KQNCX039. Recommended for publication by Associate Editor D. Qiu. *(Corresponding author: Si-Zhe Chen.)*

G. Zhang, Z. Wang, S.-Z. Chen, Y. Ye, and Y. Zhang are with the School of Automation, Guangdong University of Technology, Guangzhou 510006, China (e-mail: guidong.zhang@gdut.edu.cn; 2111604018@mail2.gdut.edu.cn; cszscut@126.com; eeyeym@gdut.edu.cn; yz@gdut.edu.cn).

H. H.-C. Iu is with the School of Electrical, Electronics and Computer Engineering, The University of Western Australia, Perth, WA 6009, Australia (e-mail: herbert.iu@uwa.edu.au).

B. Zhang is with the School of Electric Power, South China University of Technology, Guangzhou 510640, China (e-mail: epbzhang@scut.edu.cn).

Color versions of one or more of the figures in this paper are available online at http://ieeexplore.ieee.org.

Digital Object Identifier 10.1109/TPEL.2017.2770149

TABLE II
CELLS CONNECTIONS

Type	Structure	Feature
Cascaded	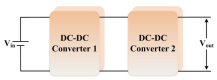	• Easy Realization • Seperate Control • Many Switches • High Cost • Complex Control • Large Size • High Cost
Output Series	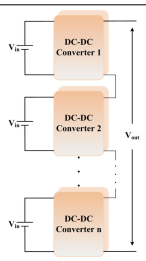	• High Power Level • High Voltage Level • Few Magnetic Component • Many Components • High Cost • Complex Control • Large Size
Interleaved	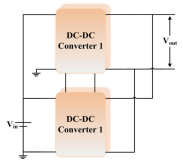	• Low Current Ripple • High Power Density • High Cost • Difficult Realization • Instability
Multi-cell	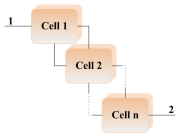	• Simple Structure • Low Loss • High Power Density • Easy Realization • Simple Control

Therein, switched-capacitor and switched-inductor techniques are widely used. In detail, switched-capacitor ones are the most popular one. For example, Cortez proposed a three-phase multilevel hybrid switched-capacitor pulse width modulation (PWM) pfc-power factor correction (PFC) rectifier with a high voltage gain [18], Zhou *et al.* devised switched-capacitor-based current compensator for mitigating the effect of long cable between PWM driver and led light source [3], and Wu *et al.* developed a family of two-switch boosting switched-capacitor converters [12], to list just a few. However, due to the low lifetime of electrolytic capacitors, the application of the switched-capacitor technique is hindered. There are also a lot of published works about switched-inductor techniques, while the multicell switched inductor is the most typical one [23], [24]. It is known that this technique is, however, limited by increasing component current stresses, which finally results in high cost, high loss, and low stability [25], [26].

In face of the existing background, this paper aims to propose a unique modular structure, which can be utilized in high-step-up converters to replace the traditional multicell switched inductor (TnSL) converters, the new designed one can not only realize higher actual voltage gain, but also reduce diode currents.

The body of this paper is organized as follows. The TnSL modular structure will be analyzed in Section II to demonstrate their shortages. Then, the proposed unique modular structure is introduced in Section III to coin out its unique features. Section IV gives a detailed comparison, including the main features, actual voltage gains, and efficiencies. To verify the effectiveness, simulations and experiments are presented in Sections V and VI, respectively. Finally, a conclusion is drawn in Section VII.

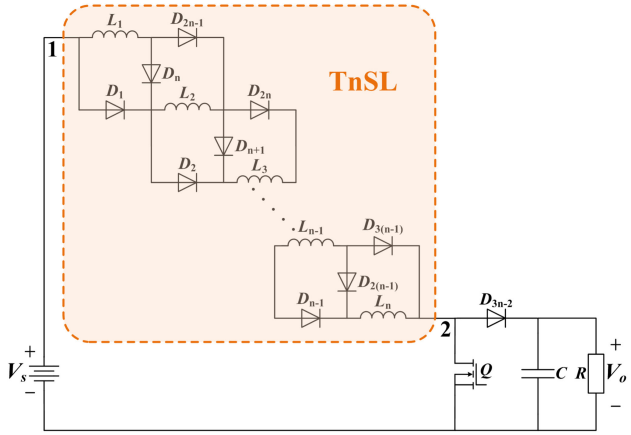

Fig. 1. Schematic of a TnSL-Boost converter.

II. TRADITIONAL MULTICELL SWITCHED INDUCTOR

Techniques of multicell connections and switched-inductor (SL) cells are combined to form the TnSL. It is a fact that the more cells are, the higher voltage gain it obtains; however, the component current stresses are dramatically increasing with the increasing number of cells, which will finally result in high cost, high loss, and low stability. This is a main reason hindering the development of TnSL in industrial applications. In the following contents, TnSL will be introduced and analyzed in detail.

A. Operational Analysis

The structure of TnSL cell is shown as the dash diagram of Fig. 1, while Fig. 1 is a schematic of a TnSL cell applying in a boost converter. Therein, TnSL is consisted of n inductors sharing the same inductance, i.e., $L_1, \ldots, L_n$, and $3(n-1)$ diodes, i.e., $D_1, \ldots, D_{3(n-1)}$.

In the steady states of a TnSL boost converter, there are two continuous-conduction modes (CCMs) corresponding to two equivalent circuits, as shown in Fig. 2(a) and (b). Therein, different colors are marked in the circuit to demonstrate different levels of current stresses.

Denote d as duty cycle of switch Q, and t_0, t_1, and t_2 as the beginning of one period, the mode transition instant from Mode 1 to Mode 2, and the end of the period, respectively. Fig. 3 depicts the key waveforms in CCM, therein, v_g is the driving voltage of switch Q; $i_{L_1}(=i_{L_2}=\cdots=i_{L_n})$ is the current of $L_1(L_2, \ldots, L_n)$; $i_{D_1}(=i_{D_{3(n-1)}})$, $i_{D_2}(=i_{D_{3n-4}})$,..., and $i_{D_{n-1}}(=i_{D_{2n-1}})$, are currents of $D_1(D_{3(n-1)})$, $D_2(D_{3n-4})$,..., and $D_{n-1}(D_{2n-1})$, respectively; and $i_{D_n}(=...=i_{D_{2(n-1)}})$ is current of $D_n(...,D_{2(n-1)})$. In order to describe the increasing diode currents, their waveforms lines are marked with corresponding colors, it is obvious that $i_{D_1}(=i_{D_{3(n-1)}})$ is dramatically increasing with the increasing n.

1) Mode 1 ($t_0 \le t < t_1$): As shown in Fig. 2(a), when Q turns ON, the corresponding diodes turn ON and OFF,as presented

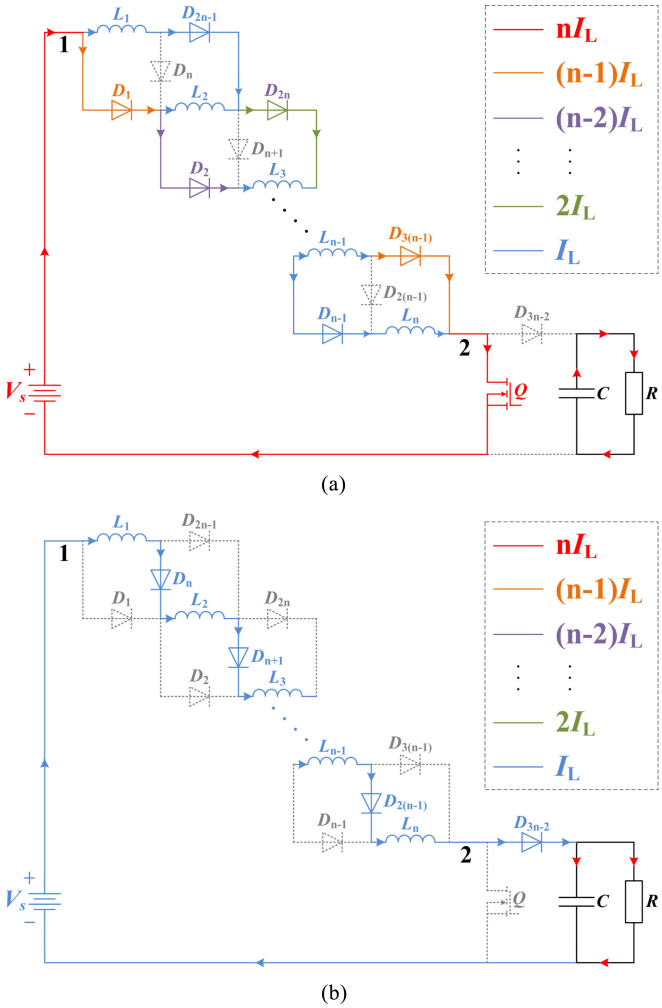

Fig. 2. Equivalent circuits of Q being (a) ON and (b) OFF.

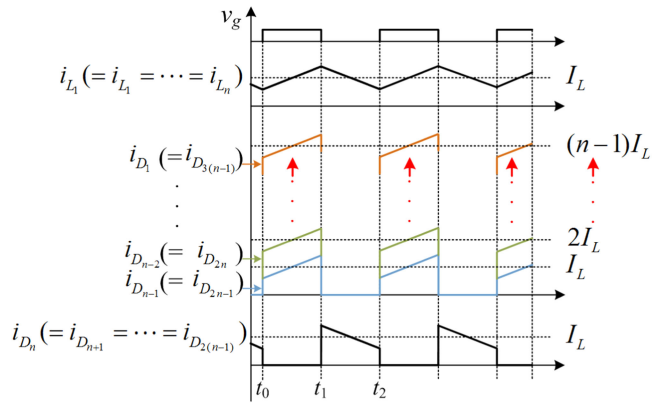

Fig. 3. Key waveforms of a TnSL-Boost converter.

in Table III, and the corresponding waveforms are shown in Fig. 3. Inductors, $L_1, L_2, \ldots, L_n$, store energy in parallel from dc source, and their voltages are

$$v_{L_1} = v_{L_2} = \cdots = v_{L_n} = V_s \tag{1}$$

TABLE III
SWITCH STATE

Switches	Mode 1	Mode 2
Q	ON	OFF
$D_1, D_2, \ldots, D_{n-1}$	ON	OFF
$D_n, D_{n+1}, \ldots, D_{2(n-1)}$	OFF	ON
$D_{2n-1}, D_{2n}, \ldots, D_{3(n-1)}$	ON	OFF
D_{3n-2}	OFF	ON

where $v_{L_1}, v_{L_2}, \ldots, v_{L_n}$ and V_s, are voltages of $L_1, L_2, \ldots, L_n$ and dc input source, respectively.

2) Mode 2 ($t_1 \le t < t_2$): As shown in Fig. 2(b), when Q turns OFF, the corresponding diodes turn ON and OFF, as presented in Table III, and the corresponding waveforms are shown in Fig. 3. All inductors are in series to boost the input voltage as

$$v_{L_1} + v_{L_2} + \ldots + v_{L_n} = V_s - V_o. \tag{2}$$

From an inductor's voltage-second constant theory yields

$$dV_s + \left(1-d\right)\frac{V_s - V_o}{n} = 0 \tag{3}$$

solve it and one can obtain voltage gain of TnSL-Boost as

$$G_{\mathrm{TnSL}} = \frac{V_o}{V_s} = \frac{(n-1)d+1}{1-d}. \tag{4}$$

B. Shortages of TnSL

In this section, shortages of TnSL will be analyzed. As shown in Fig. 3 and corresponding color lines of Fig. 2, it is clear that diode currents are increasing with the cells number n. Specially, the largest one will bear $n-1$ times of inductor currents, which implies high cost of diodes.

Assume $L_1 = L_2 = \cdots = L_n$ and all inductances are large enough to have constant currents, one has

$$i_{L_1} = i_{L_2} = \cdots = i_{L_n} = I_L \tag{5}$$

where I_L is the current of inductors.

Then, the diode currents can be derived as

$$\begin{cases} i_{D_{n-1}} = i_{L_n} = I_L, \\ i_{D_{n-2}} = i_{L_n} + i_{L_{n-1}} = 2I_L, \\ i_{D_{n-3}} = i_{L_n} + i_{L_{n-1}} + i_{L_{n-2}} = 3I_L, \\ \quad\vdots \\ i_{D_1} = i_{L_n} + i_{L_{n-1}} + \cdots + i_{L_2} = (n-1)I_L \end{cases} \tag{6}$$

and

$$\begin{cases} i_{D_{2n-1}} = i_{L_1} = I_L, \\ i_{D_{2n}} = i_{L_1} + i_{L_2} = 2I_L, \\ i_{D_{2n+1}} = i_{L_1} + i_{L_2} + i_{L_3} = 3I_L, \\ \quad\vdots \\ i_{D_{3(n-1)}} = i_{L_1} + i_{L_2} + \cdots + i_{L_{n-1}} = (n-1)I_L. \end{cases} \tag{7}$$

As shown in (6) and (7) of Mode 1, $D_1, \ldots, D_{n-2}$ and $D_{2n}, \ldots, D_{3(n-1)}$ bear more than one time of I_L, which will finally result in high conduction losses and low voltage gain, moreover, the conditions will become worse as the number of

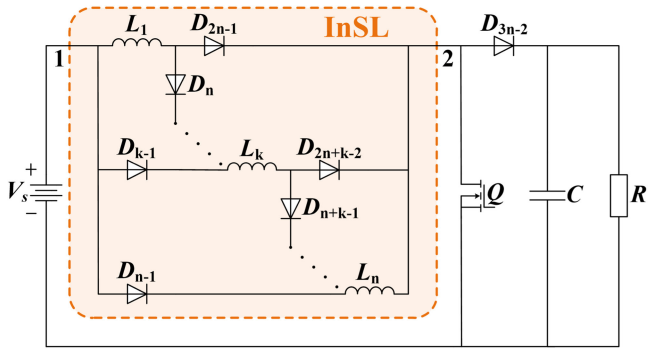

Fig. 4. Schematic of an InSL-Boost converter.

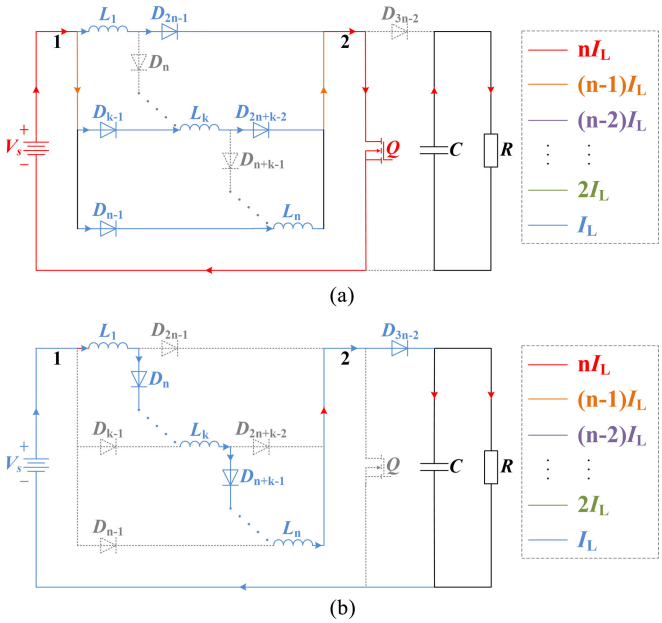

Fig. 5. Equivalent circuits of Q being (a) ON and (b) OFF.

cells increase. The corresponding current stresses have been marked with different colors in Fig. 2(a).

III. Improved Multicell Switched Inductor (InSL)

As shown in the dash diagram of Fig. 4, a novel InSL is devised to overcome shortages of TnSL, while Fig. 4 depicts the InSL modular structure applied in a boost converter as an example, namely InSL-boost converter (InSL-Boost). Similarly, InSL has the same components as TnSL but with different structure. Compared to the traditional one, the proposed one can not only achieve higher voltage gain, but also reduced diode currents, i.e., the diode currents are only one time of I_L even with the increasing number of cells. The detailed analysis is presented as follows.

A. Operational Analysis

In steady states, InSL-Boost corresponds to two equivalent circuits of CCMs, as shown in Fig. 5, while the corresponding waveforms are depicted in Fig. 6. Therein, corresponding

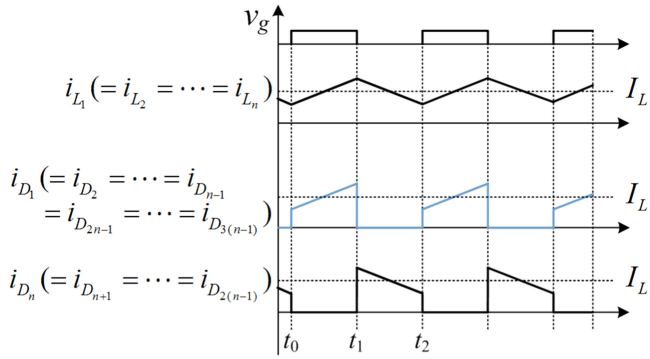

Fig. 6. Key waveforms of an InSL-Boost converter.

TABLE IV
Comparison of InSL-Boost and TnSL-Boost

	TnSL-Boost	InSL-Boost
G	$\frac{(n-1)d+1}{1-d}$	$\frac{(n-1)d+1}{1-d}$
I_L	$\frac{V_o}{(1-d)R}$	$\frac{V_o}{(1-d)R}$
$v_{D_{n-1}}$ and $v_{D_{2n-1}}$	$\frac{(V_o-V_s)}{n}$	$\frac{(n-1)(V_o-V_s)}{n}$
$v_{D_{n-2}}$ and $v_{D_{2n}}$	$\frac{(V_o-V_s)}{n}$	$\frac{(n-2)(V_o-V_s)}{n}$
⋮	⋮	⋮
v_{D_1} and $v_{D_{3(n-1)}}$	$\frac{(V_o-V_s)}{n}$	$\frac{(V_o-V_s)}{n}$
$v_{D_{(3n-2)}}$	V_o	V_o
$i_{D_{(3n-2)}}$	I_L	I_L

parameters are as the ones of TnSL. Similarly, the analysis is presented as follows.

1) Mode 1 ($t_0 \le t < t_1$): As depicted in Fig. 5(a), switch Q is ON. The switch states are the same as the ones presented in Table III. The inductors store energy in parallel from the dc source, and the corresponding voltages are

$$v_{L_1} = v_{L_2} = \cdots = v_{L_n} = V_s. \tag{8}$$

2) Mode 2 ($t_1 \le t < t_2$): As shown in Fig. 5(b), switch Q turns OFF, and the switch states are the same as the ones presented in Table III. The inductors are in series and one has

$$v_{L_1} + v_{L_2} + \cdots + v_{L_n} = V_s - V_o \tag{9}$$

which results in

$$dV_s + \left(1-d\right)\frac{V_s - V_o}{n} = 0 \tag{10}$$

solve it and one has the same voltage gain of TnSL as

$$G_{\mathrm{InSL}} = \frac{V_o}{V_s} = \frac{(n-1)d+1}{1-d}. \tag{11}$$

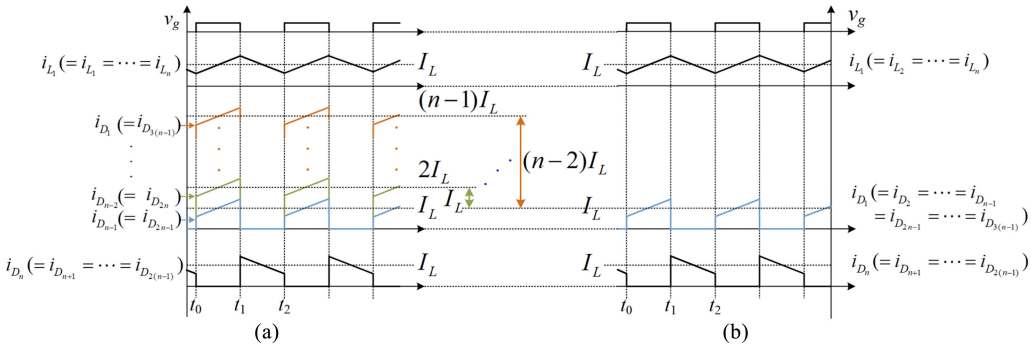

Fig. 7. Waveforms comparison of (a) TnSL-Boost and (b) InSL-Boost.

B. Diode Current

As shown in Figs. 5 and 6, the corresponding diode currents are marked with different colors, and the corresponding color represents one current stress that is labeled in figures. It is clear that diode currents in InSL are only one time of I_L even with the increasing number of cells, but the ones of TnSL increase with increasing n.

IV. Comparison Analysis

In order to demonstrate the features of the proposed structure, performance comparisons of TnSL-Boost and InSL-Boost are conducted in this section.

A. Main Parameters

In detail, the main parameter are demonstrated in Table IV with comparison of voltage gains, inductor currents, diode currents, and diode reverse voltages. Moreover, key waveforms are also compared in Fig. 7. It is noted that InSL-Boost has lower diode currents and condition loss than TnSL-Boost according to Table IV and Fig. 7.

According to Zhang *et al.* [11], the parameters design can be obtained by expressions presented in Table IV and Fig. 7. Therefore, the detailed deductions are not presented here due to the page limitations.

B. Voltage Gain Considering Parasitic Parameters

It is known that parasitic parameters, such as diode forward voltages (V_D), diode conduction resistors (R_D), winding resistors of inductors (R_L), and the drain–source on-resistance ($R_{\rm DS}$), have effects on gain and efficiency. For example, although the ideal gains of T4SL-Boost and I4SL-Boost are same, their actual voltage gains are different if parasitic parameters are considered. In detail, the corresponding equivalent circuits and voltage gain equations are compared in Table V, therein, $a_{\rm T}=n+n(nd-2d)>a_{\rm I}=n+(nd-2d)$, and $b_{\rm T}=n+(nd-2d)(n^2+n)/2>b_{\rm I}=n+(nd-2d)$. Since the other variables are same, it can be deduced that $G_{\rm InSL}>G_{\rm TnSL}$. It is forwarded with typical voltage gains of a traditional four-cell switched-inductor boost (T4SL-Boost) and an improved four-cell switched-inductor boost (I4SL-Boost), substitute their parameters, $n=4$, $V_s=20$ V, $V_D=0.4$–0.6 V (decided by different diodes), $R_D=50\,\text{m}\Omega$, $R_L=200\,\text{m}\Omega$, and $R_{\rm DS}=110\,\text{m}\Omega$, into Table V, and one can obtain their voltage gain curves, as shown in Fig. 8. It is remarked that one of I4SL-Boost is obvious higher than that of T4SL-Boost.

C. Efficiency Considering Parasitic Parameters

Similarly, their efficiencies considering parasitic parameters are discussed as follows:

$$\eta=\frac{P_o}{P_o+P_{\rm loss}}=\frac{V_o^2/R}{V_o^2/R+P_L+P_D+P_S+P_C} \tag{12}$$

where $P_o=V_o^2/R$ and $P_{\rm loss}=P_L+P_D+P_S+P_C$ are the output power and power loss of the converter, respectively. Therein, P_L, P_D, P_S, and P_C are power loss of inductors, diodes, switch, and capacitor, respectively, and their expressions are shown as follows:

$$P_L=nI_L^2R_L \tag{13}$$

where I_L and R_L are the rms current of inductor and the winding inductor resistor, respectively

$$P_D=\sum_{k=1}^{3n-2}\left(I_{D_{k\,(\rm av)}}V_D+I_{D_k}^2R_D\right) \tag{14}$$

where $I_{D_{k\,(\rm av)}}$ and I_{D_k} are the average and rms currents of diode, respectively

$$\begin{aligned}P_S&=P_{Q(\rm con)}+P_{Q(\rm swi)}\\&=I_S^2R_{\rm DS}+\frac{\left(V_{\rm DS(off)}I_{S(\rm on)}(t_{\rm on}+t_{\rm off})\right)f_s}{6}\end{aligned} \tag{15}$$

where $P_{Q(\rm con)}$ and $P_{Q(\rm swi)}$ are conduction and switching power losses of Q, respectively; I_S is the rms current of Q; $V_{\rm DS(off)}$, $I_{S(\rm on)}$, $t_{\rm on}$, and $t_{\rm off}$ are the drain–source voltage of Q being OFF, current of Q being ON, turn-on-transient and the turn-off-transient time intervals of Q, respectively

$$P_C=I_C^2R_C \tag{16}$$

where I_C is the rms current of C.

Similarly, T4SL-Boost and I4SL-Boost are discussed as examples, substitute parameters, $n=4$, $V_D=0.4$–0.6 V (decided by different diodes), $R_D=50\,\text{m}\Omega$, $R_L=200\,\text{m}\Omega$, $R_C=200\,\text{m}\Omega$, $R_{\rm DS}=110\,\text{m}\Omega$, $t_{\rm on}=54$ ns, and $t_{\rm off}=125$ ns, into

TABLE V
ACTUAL GAIN COMPARISON

Equivalent Circuits with parasitic parameters	Actual gain
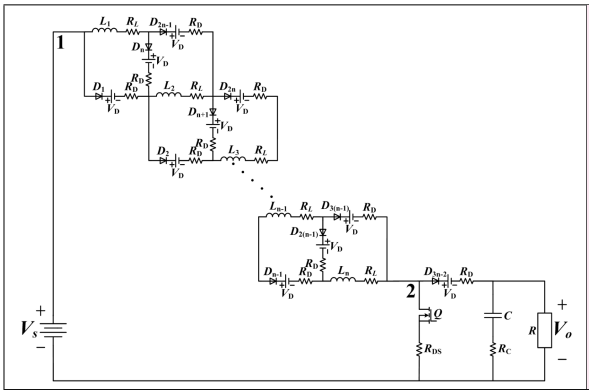	$G_{\mathrm{TnSL}} = \dfrac{((n-1)d+1) - a_{\mathrm{T}} \cdot \dfrac{V_D}{V_S}}{(1-d) + \dfrac{nR_L + n^2 dR_{DS} + b_{\mathrm{T}} \cdot R_D}{(1-d)R}}$
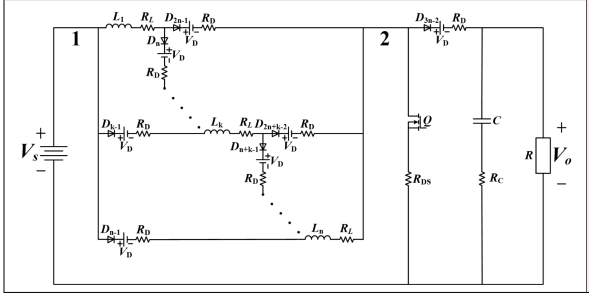	$G_{\mathrm{InSL}} = \dfrac{((n-1)d+1) - a_{\mathrm{I}} \cdot \dfrac{V_D}{V_S}}{(1-d) + \dfrac{nR_L + n^2 dR_{DS} + b_{\mathrm{I}} \cdot R_D}{(1-d)R}}$

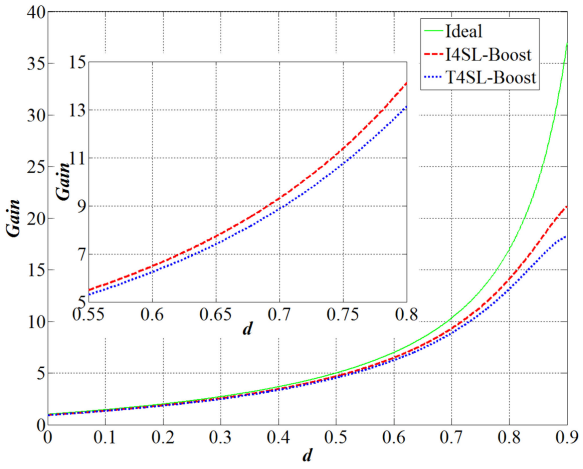

Fig. 8. Voltage gain comparison.

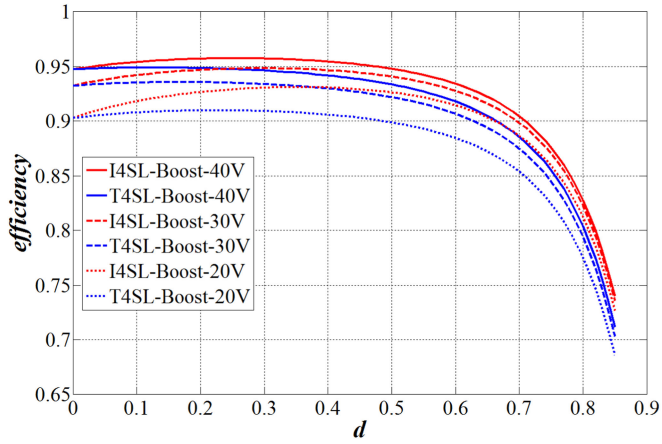

Fig. 9. Efficiency curves of $V_s = 40$, 30, and 20 V.

(12), and one can plot their curves, as shown in Fig. 9. With the same input voltage, the efficiency of I4SL-Boost is higher than the ones of T4SL-Boost in all conditions. Assume their output powers $P_o = 100$ W, their different parts of losses are compared in Fig. 10. It is remarked that diode power loss of T4SL is larger than the ones of I4SL, which finally raises higher efficiency of I4SL.

V. SIMULATIONS VERIFICATIONS

In order to verify the effectiveness of the proposed modular structure, four-cells of TnSL- and InSL-Boost converters are simulated, and their schematics are shown in Figs. 11 and 12, respectively. Assume the corresponding parameters depicted in Table VI, and simulation results via PSIM software are depicted in Fig. 13(a) and (b). It is remarked that the results agree with the theoretical analysis.

VI. EXPERIMENTS VERIFICATIONS

Two prototypes with corresponding parameters, presented in Table VII, are built as shown in Fig. 14 and tested under conditions given in Table VIII. According to Table VII, it is found that in the same experimental conditions, rated currents of D_1, D_2, D_8, and D_9 in I4SL-Boost are lower than the ones of T4SL-Boost. Then, one can obtain experimental results as:

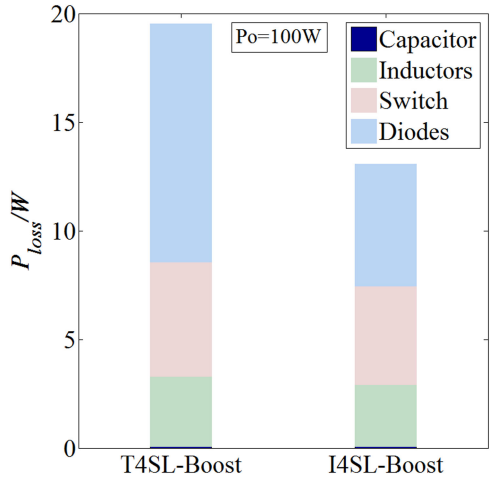

Fig. 10. Power loss comparison of $V_s = 20$ V.

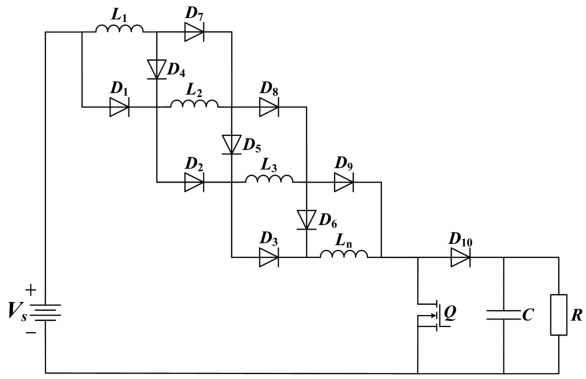

Fig. 11. Traditional four-cell switched-inductor boost converter.

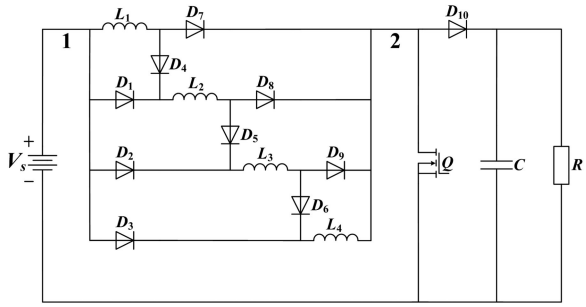

Fig. 12. I4SL-Boost converter.

TABLE VI
SIMULATIONS PARAMETERS

V_s	f	$L_1, L_2, ..., L_4$	C	R
20 V	50 kHz	330 μH	330 μF	200 Ω

1) Figs. 15(a) and 16(a) demonstrate waveforms of v_{GS}, v_{DS}, V_s, and V_o;

2) while Figs. 15(b) and 16(b) depict waveforms of i_{L_1}, i_{L_2}, and i_{L_3}; and

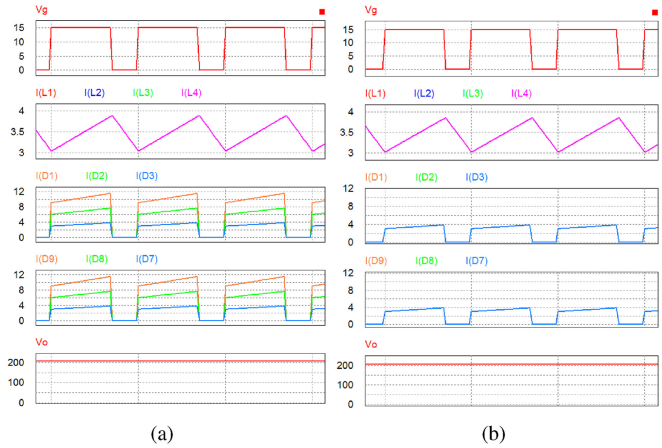

Fig. 13. Simulation waveforms of (a) T4SL-Boost and (b) I4SL-Boost.

TABLE VII
EXPERIMENTAL PARAMETERS

Parameters	T4SL-Boost	I4SL-Boost
Input voltage V_s	20 V	20 V
Output voltage V_o	200 V	200 V
Output power P_o	100 W	100 W
Switching frequency f_s	50 kHz	50 kHz
Inductors $L_1, \ldots, L_4$	470 μH	470 μH
MOSFET Q	IXTQ36N30P	IXTQ36N30P
Driving IC	IXDN404SIA	IXDN404SIA
Diodes D_1 and D_9	8TQ100	SS36
Diodes D_2 and D_8	SS56	SS310
Diodes D_3 and D_7	SS36	SS3200
Diodes D_4, D_5, and D_6	SS36	SS36
Diode D_{10}	HER304	HER304
Capacitor C	330 μF/250 V	330 μF/250 V

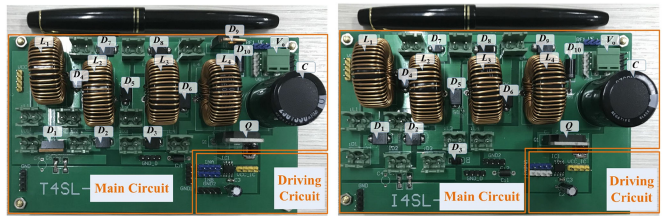

Fig. 14. Prototypes of (a) T4SL-Boost and (b) I4SL-Boost.

3) Figs. 15(c), 16(c), 15(d), and 16(d) remark that i_{D_1}, i_{D_2}, i_{D_8}, and i_{D_9} of I4SL-Boost are lower than the ones of T4SL-Boost.

In order to verify the advancements of InSL in actual voltage gain and efficiency, experimental and theoretical results are plotted and compared in Figs. 17 and 18. In detail, Fig. 17 depicts their actual voltage gain curves when $V_s = 20$ V with a plugged output voltage comparison table, whereas Fig. 18 shows the experimental efficiency measurement curves of $V_s = 40$, 30, 20 V with plugging efficiency data subtables, which shows that the highest experimental efficiency of an

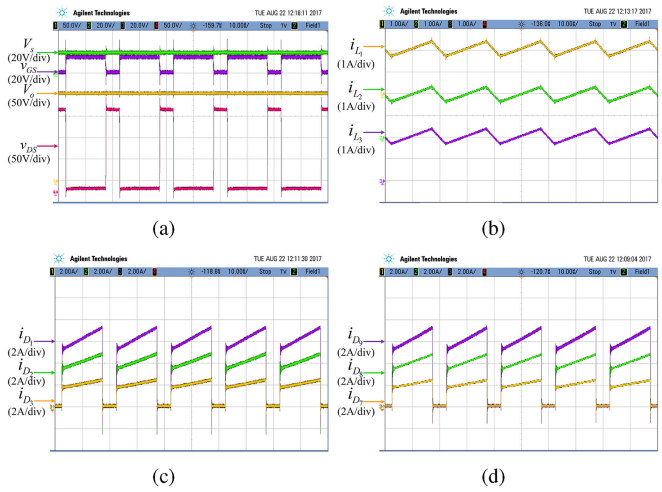

Fig. 15. Experimental waveforms of T4SL-Boost.

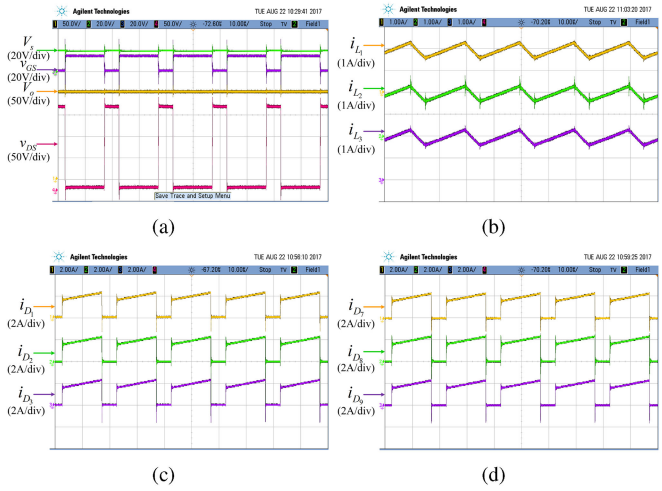

Fig. 16. Experimental waveforms of I4SL-Boost.

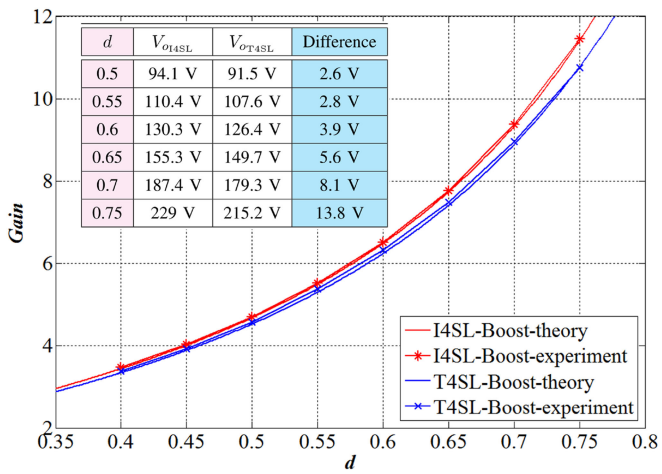

d	V_{oI4SL}	V_{oT4SL}	Difference
0.5	94.1 V	91.5 V	2.6 V
0.55	110.4 V	107.6 V	2.8 V
0.6	130.3 V	126.4 V	3.9 V
0.65	155.3 V	149.7 V	5.6 V
0.7	187.4 V	179.3 V	8.1 V
0.75	229 V	215.2 V	13.8 V

Fig. 17. Theory and experiment voltage gain comparisons.

TABLE VIII
EXPERIMENTAL PLATFORM

DC Power Supply	Oscilloscope	Current Probe	Control Unit
KIKUSUI PWR800L	Agilent DSO7104A	Agilent 1147A	STM32F103ZET6

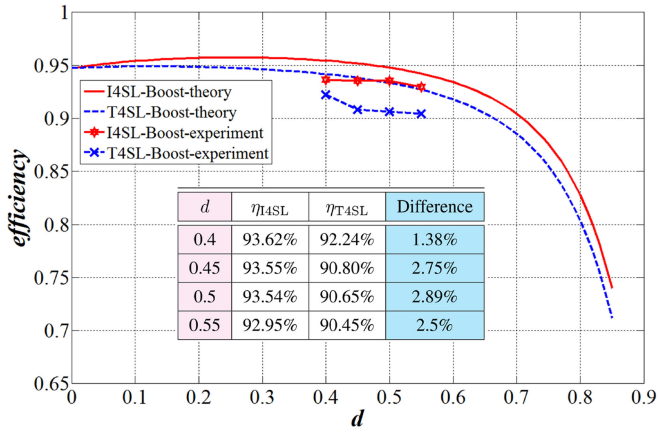

d	η_{I4SL}	η_{T4SL}	Difference
0.4	93.62%	92.24%	1.38%
0.45	93.55%	90.80%	2.75%
0.5	93.54%	90.65%	2.89%
0.55	92.95%	90.45%	2.5%

(a)

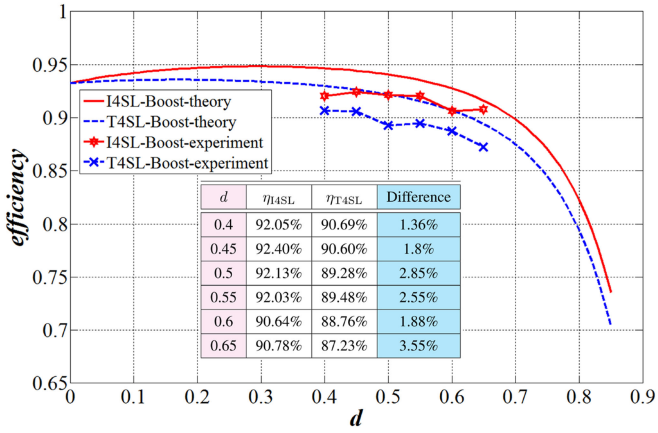

d	η_{I4SL}	η_{T4SL}	Difference
0.4	92.05%	90.69%	1.36%
0.45	92.40%	90.60%	1.8%
0.5	92.13%	89.28%	2.85%
0.55	92.03%	89.48%	2.55%
0.6	90.64%	88.76%	1.88%
0.65	90.78%	87.23%	3.55%

(b)

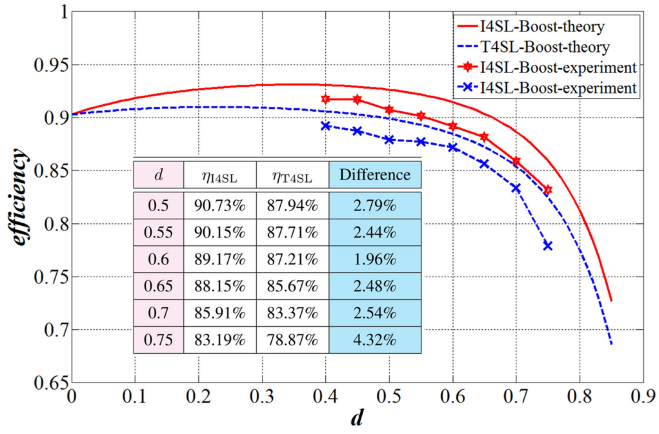

d	η_{I4SL}	η_{T4SL}	Difference
0.5	90.73%	87.94%	2.79%
0.55	90.15%	87.71%	2.44%
0.6	89.17%	87.21%	1.96%
0.65	88.15%	85.67%	2.48%
0.7	85.91%	83.37%	2.54%
0.75	83.19%	78.87%	4.32%

(c)

Fig. 18. Efficiencies of theory and experiment: (a) $V_s = 40$ V, (b) $V_s = 30$ V, and (c) $V_s = 20$ V.

I4SL-Boost converter is about 94%, and the largest efficiency difference between InSL-Boost and TnSL-Boost is 4.32%. There is only about 1.5% difference between the efficiencies of theory analysis and experimental tests, which implies that the theory analysis is consistent with the experiments. Moreover, the tiny difference is also reasonable since some tiny losses are ignored here, e.g., the core losses of inductors and the switching losses of diodes. It is concluded that experimental results are consistent with simulations and theoretical analysis, i.e., I4SL-Boost is superior to T4SL-Boost both in efficiency and actual voltage gain, which forwardly implies that the InSL modular structure had unique features to replace TnSL in industrial applications.

VII. Conclusion

This paper has devised a novel multicell modular topology based on switched-inductor techniques. Compared to the traditional multi-cell one, the proposed one can achieve higher actual voltage gain with the same components but reduce diode currents even with the increasing number of cells, which finally reduces its power losses and economy costs. In detail, their main parameters, actual voltage gains, and efficiencies considering parasitic parameters are described in detail. Two experimental prototypes are built to validate the advancements of the proposed structure, it is found that the proposed structure has higher efficiency and lower diode currents compared to the traditional ones, the highest efficiency of I4SL-Boost can realize about 94%, and the largest efficiency difference between InSL-Boost and TnSL-Boost is 4.32%. Therefore, the proposed structure can be used in high-voltage converters to replace the traditional one.

References

[1] M. Forouzesh, Y. P. Siwakoti, S. A. Gorji, F. Blaabjerg, and B. Lehman, "Step-up DC–DC converters: A comprehensive review of voltage boosting techniques, topologies, and applications," *IEEE Trans. Power Electron.*, vol. 32, no. 12, pp. 9143–9178, Dec. 2017.

[2] Y. Tang, D. Fu, T. Wang, and Z. Xu, "Hybrid switched-inductor converters for high step-up conversion," *IEEE Trans. Ind. Electron.*, vol. 62, no. 3, pp. 1480–1490, Mar. 2015.

[3] R. Zhou, R. S.-C. Yeung, J. Y.-C. Chan, N. C.-F. Tse, and H. S.-H. Chung, "Switched-capacitor-based current compensator for mitigating the effect of long cable between PWM driver and led light source," *IEEE Trans. Power Electron.*, 2017, to be published.

[4] G. Zhang, B. Zhang, and Z. Li, *Designing Impedance Networks Converters*. Springer, 2017.

[5] X. Hu and C. Gong, "A high gain input-parallel output-series DC/DC converter with dual coupled inductors," *IEEE Trans. Power Electron.*, vol. 30, no. 3, pp. 1306–1317, Mar. 2015.

[6] G. Zhang, Z. Li, B. Zhang, and W. A. Halang, "Power electronics converters: Past, present and future," *Renew. Sustain. Energy Rev.*, to be published.

[7] S. Li, K. W. E. Cheng, Y. Ye, and Z. Shi, "Wide input and wide output topology analysis for tapped-inductor converters with consideration of parasitic elements," *IET Power Electron.*, vol. 9, no. 9, pp. 1952–1961, 2016.

[8] K.-C. Tseng and C.-C. Huang, "High step-up high-efficiency interleaved converter with voltage multiplier module for renewable energy system," *IEEE Trans. Ind. Electron.*, vol. 61, no. 3, pp. 1311–1319, Mar. 2014.

[9] G. Zhang *et al.*, "An impedance network boost converter with a high-voltage gain," *IEEE Trans. Power Electron.*, vol. 32, no. 9, pp. 6661–6665, 2017.

[10] Y. P. Siwakoti and F. Blaabjerg, "Single switch nonisolated ultra-step-up DC–DC converter with an integrated coupled inductor for high boost applications," *IEEE Trans. Power Electron.*, vol. 32, no. 11, pp. 8544–8558, Nov. 2017.

[11] G. Zhang, B. Zhang, Z. Li, D. Qiu, L. Yang, and W. A. Halang, "A 3-z-network boost converter," *IEEE Trans. Ind. Electron.*, vol. 62, no. 1, pp. 278–288, Jan. 2015.

[12] B. Wu, S. Li, K. M. Smedley, and S. Singer, "A family of two-switch boosting switched-capacitor converters," *IEEE Trans. Power Electron.*, vol. 30, no. 10, pp. 5413–5424, Oct. 2015.

[13] Y. Yang, P. Enjeti, F. Blaabjerg, and H. Wang, "Wide-scale adoption of photovoltaic energy: Grid code modifications are explored in the distribution grid," *IEEE Ind. Appl. Mag.*, vol. 21, no. 5, pp. 21–31, Sep./Oct. 2015.

[14] Y. P. Siwakoti, F. Z. Peng, F. Blaabjerg, P. C. Loh, and G. E. Town, "Impedance-source networks for electric power conversion part I: A topological review," *IEEE Trans. Power Electron.*, vol. 30, no. 2, pp. 699–716, Feb. 2015.

[15] Y. P. Siwakoti, F. Z. Peng, F. Blaabjerg, P. C. Loh, G. E. Town, and S. Yang, "Impedance-source networks for electric power conversion part II: Review of control and modulation techniques," *IEEE Trans. Power Electron.*, vol. 30, no. 4, pp. 1887–1906, Apr. 2015.

[16] Y. P. Siwakoti, P. C. Loh, F. Blaabjerg, S. J. Andreasen, and G. E. Town, "Y-source boost DC/DC converter for distributed generation," *IEEE Trans. Ind. Electron.*, vol. 62, no. 2, pp. 1059–1069, Feb. 2015.

[17] J. E. Huber and J. W. Kolar, "Optimum number of cascaded cells for high-power medium-voltage AC–DC converters," *IEEE J. Emerg. Sel. Topics Power Electron.*, vol. 5, no. 1, pp. 213–232, Mar. 2017.

[18] D. F. Cortez and I. Barbi, "A three-phase multilevel hybrid switched-capacitor PWM PFC rectifier for high-voltage-gain applications," *IEEE Trans. Power Electron.*, vol. 31, no. 5, pp. 3495–3505, May 2016.

[19] Y.-T. Chen, T.-M. Li, and R.-H. Liang, "A novel soft-switching interleaved coupled-inductor boost converter with only single auxiliary circuit," *IEEE Trans. Power Electron.*, to be published.

[20] W. Li, W. Li, X. Xiang, Y. Hu, and X. He, "High step-up interleaved converter with built-in transformer voltage multiplier cells for sustainable energy applications," *IEEE Trans. Power Electron.*, vol. 29, no. 6, pp. 2829–2836, Jun. 2014.

[21] F. Forest *et al.*, "A non-reversible 10 kW high step-up converter using a multi-cell boost topology," *IEEE Trans. Power Electron.*, vol. 33, no. 1, pp. 151–160, 2018.

[22] Y. Tang, T. Wang, and D. Fu, "Multicell switched-inductor/switched-capacitor combined active-network converters," *IEEE Trans. Power Electron.*, vol. 30, no. 4, pp. 2063–2072, Apr. 2015.

[23] D. Li, P. C. Loh, M. Zhu, F. Gao, and F. Blaabjerg, "Generalized multicell switched-inductor and switched-capacitor Z-source inverters," *IEEE Trans. Power Electron.*, vol. 28, no. 2, pp. 837–848, Feb. 2013.

[24] A.-V. Ho, T.-W. Chun, and H.-G. Kim, "Extended boost active-switched-capacitor/switched-inductor quasi-Z-source inverters," *IEEE Trans. Power Electron.*, vol. 30, no. 10, pp. 5681–5690, Oct. 2015.

[25] M.-K. Nguyen, Y.-C. Lim, S.-J. Park, and D.-S. Shin, "Family of high-boost Z-source inverters with combined switched-inductor and transformer cells," *IET Power Electron.*, vol. 6, no. 6, pp. 1175–1187, 2013.

[26] A.-V. Ho, T.-W. Chun, and H.-G. Kim, "Development of multi-cell active switched-capacitor and switched-inductor z-source inverter topologies," *J. Power Electron.*, vol. 14, no. 5, pp. 834–841, 2014.

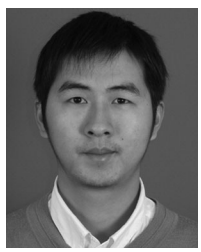

Guidong Zhang (M'13) was born in Guangdong, China, in 1986. He received the B.Sc. degree from Xi'an University of Technology, Xi'an, China, in 2008, and two Ph.D. degrees from the South China University of Technology, Guangzhou, China, in 2014, and FernUniversität, Hagen, Germany, in 2015, respectively.

He is currently an Associate Professor with the School of Automation, Guangdong University of Technology, Guangzhou, China. His research interests include power electronics topology and their applications.

Zhiyang Wang was born in Jiangxi, China, in 1994. He received the B.Sc. degree in electrical engineering from Chongqing University of Technology, Chongqing, China, in 2016. He is currently working toward the M.Sc. degree in electrical engineering from the School of Automation, Guangdong University of Technology, Guangzhou, China.

He is a visiting student at the School of Electrical, Electronic and Computer Engineering, The University of Western Australia, Perth, Australia. His current research interests include power electronics topology and their applications.

Herbert Ho-Ching Iu (M'00–SM'06) received the B.Eng. (Hons.) degree in electrical and electronic engineering from the University of Hong Kong, Hong Kong, in 1997 and the Ph.D. degree from the Hong Kong Polytechnic University, Hong Kong, in 2000. In 2002, he joined the School of Electrical, Electronic and Computer Engineering, The University of Western Australia, where he is currently a Professor. His research interests include power electronics, renewable energy, nonlinear dynamics, current sensing techniques, and memristive systems.

Dr. Ho-Ching lu is currently an Associate Editor for the IEEE TRANSACTIONS ON POWER ELECTRONICS, the IEEE TRANSACTIONS ON SMART GRIDS, the IEEE TRANSACTIONS ON NETWORK SCIENCE AND ENGINEERING, the IEEE TRANSACTIONS ON CIRCUITS AND SYSTEMS-II, and IEEE ACCESS.

Si-Zhe Chen was born in Shantou, Guangdong, China, in 1981. He received the B.Sc. in mechatronic engineering and Ph.D. degree in control theory and control engineering from the South China University of Technology, Guangzhou, China, in 2005 and 2010, respectively. He currently is an associate professor in the School of Automation, Guangdong University of Technology, Guangzhou, China.

His general research interests include the control and power electronics technology in renewable energy.

Yuanmao Ye (M'17) received the B.Sc. degree in electrical engineering from University of Jinan, Jinan, China, in 2007, the M.Sc. degree in control theory and control engineering from South China University of Technology, Guangzhou, China, in 2010, and the Ph.D. degree in power electronics, from the Hong Kong Polytechnic University, Hong Kong, in 2016.

From September 2010 to January 2014, he was with the Department of Electrical Engineering, Hong Kong Polytechnic University, as a Research Assistant. He is currently a full Professor with the School of Automation, Guangdong University of Technology, Guangzhou, China. His research interests include various dc–dc power converters, switched-capacitor technique and its applications, multilevel inverters, energy storage, and management for dc microgrid.

Bo Zhang (M'03–SM'15) was born in Shanghai, China, in 1962. He received the B.S. degree in electrical engineering from Zhejiang University, Hanzhou, China, in 1982, the M.S. degree in power electronics from Southwest Jiaotong University, Chengdu, China, in 1988, and the Ph.D. degree in power electronics from Nanjing University of Aeronautics and Astronautics, Nanjing, China, in 1994.

He is currently a Professor with the School of Electric Power, South China University of Technology, Guangzhou, China. He has authored or coauthored more than 380 papers and 80 patents. His current research interests include nonlinear analysis and control of power supplies and ac drives.

Yun Zhang received the B.Sc. and M.Sc. degrees in automatic engineering from Hunan University, Changsha, China, in 1982 and 1986, respectively, and the Ph.D. degree in automatic engineering from the South China University of Technology, Guangzhou, China, in 1998.

He is currently a Professor with the School of Automation, Guangdong University of Technology, Guangzhou, China. His current research interests include intelligent control systems, network systems, and signal processing.